

Scintillation detectors constructed with an optimized 2x2 silicon photomultiplier array

Felix Liang, *Member, IEEE*, Hartmut Brands, *Member, IEEE*, Les Hoy, *Member, IEEE*,
Jeff Preston, *Member, IEEE*, and Jason Smith, *Member, IEEE*,

Abstract—Silicon photomultipliers (SiPMs) are a good alternative to photomultiplier tubes (PMTs) because their gain and quantum efficiency are comparable to PMTs. However, the largest single-chip SiPM is still less than 1 cm². In order to use SiPMs with scintillators that have reasonable sensitivity, it is necessary to use multiple SiPMs. In this work, scintillation detectors are constructed and tested with a custom 2x2 SiPM array. The layout of the SiPMs and the geometry of the scintillator were determined by performing Geant4 simulations. Cubic NaI, CsI, and CLYC with 18 mm sides have been tested. The output of the scintillation detectors are stabilized over the temperature range between -20 and 50 °C by matching the gain of the SiPMs in the array. The energy resolution for these detectors has been measured as a function of temperature. Furthermore, neutron detection for the CLYC detector was studied in the same temperature range. Using pulse-shape discrimination, neutrons can be cleanly identified without contribution from γ -photons. As a result, these detectors are suitable for deploying in spectroscopic personal radiation detectors (SPRD).

Index Terms—Geant4, silicon photomultiplier, NaI, CsI, CLYC, pulse-shape discrimination, gain stabilization, temperature, spectroscopic personal radiation detector.

I. INTRODUCTION

Silicon photomultipliers (SiPMs) are constructed on a single substrate and consist of thousands of microcells operating in the Geiger mode. The gain and quantum efficiency of the SiPMs are comparable to those of the photomultiplier tubes (PMTs). They are compact in size and insensitive to magnetic fields. With low-operating voltages, it simplifies the circuit design for electrical safety considerations. Therefore, they are a good alternative to PMTs [1]. However, the conventional PMTs are available in various sizes that are as large as a few tens of cm in diameter. In contrast, the largest single-chip SiPM is less than 1 cm². For scintillation detectors, the efficiency of scintillation photon collection increases with the area of the photon sensor. Moreover, a larger detector volume has a higher sensitivity for radiation detection. Because of the small active area of the SiPMs, it is necessary to use multiple SiPMs to increase the efficiency of photon collection for a larger scintillator. In this work, scintillation detectors are constructed and tested with a custom 2x2 SiPM array.

II. GEANT4 SIMULATIONS

The layout of the SiPM array and the geometry of the scintillator were determined by performing Geant4 simulations

Felix Liang, Hartmut Brands, Les Hoy, and Jason Smith are with FLIR Systems Inc.

Jeff Preston, formerly with FLIR Systems Inc., is now with Consolidated Nuclear Security, LLC.

[2] in which a point source is located 20 cm from the front of the scintillator. The γ -rays are emitted uniformly random in a cone irradiating a circular area inscribed by the front surface. The surface finish of the scintillator is modeled using the “groundteflonair” option in the Look-Up-Table (LUT) [3]. A thin layer of optical grease, 0.1 mm, is sandwiched between the scintillator and the SiPMs for transporting scintillation photons. The array has four 6x6 mm² SiPMs arranged in a 2x2 configuration such that the electronics is less complicated. The goal of the simulations was to find the optimum geometry of the scintillator and the layout of the SiPMs for good γ -ray energy resolution.

It is found that the energy resolution of a detector is better for the scintillator with an area comparable to the active area of the SiPM array. Since the SiPMs are arranged as a square or rectangle in the array, scintillators with a square or rectangular cross section have a better energy resolution than those with a circular cross section. Shown in Fig. 1(a) is the photon distribution at the exit surface of an 18 mm cubic scintillator. The profile of photon distribution for a 6 mm horizontal strip across the middle of the exit surface is shown in Fig. 1(b). As can be seen, more scintillation photons are distributed near the center of the exit surface of the scintillator.

For scintillators with a cross section larger than the active area of the SiPMs, leaving a gap between the SiPMs leads to a better energy resolution. In Fig. 1(c), the energy resolution for an 18 mm cubic scintillator as a function of the gap size between the active area of the SiPMs is shown. The best energy resolution is for the gap size between 1 and 2 mm. For larger gap sizes, the resolution gets worse slowly but a shoulder starts to develop on either side of the photopeak resulting in a poorer full-width-at-tenth-maximum. Fig. 2 shows the simulated 662 keV γ -ray spectra detected by the 18 mm cubic scintillator and SiPM array with the gap size of 0.2, 1.4, and 4.0 mm. It can be seen that for the gap size of 4.0 mm a noticeable shoulder appears on the high-energy side of the photopeak and the trough between the photopeak and the Compton edge is higher as well. Furthermore, the photopeak position shifts to lower channels as the gap size increases. This is due to less photons distributed away from the center of the detection plane as shown in the profile of photon distribution in Fig. 1(b). In Fig. 1(d), the gap size between the SiPMs for cubic scintillators with dimensions between 16 and 24 mm to have an optimum resolution is shown. As can be seen, it is necessary to increase the gap size for larger scintillators in order to achieve a better energy resolution.

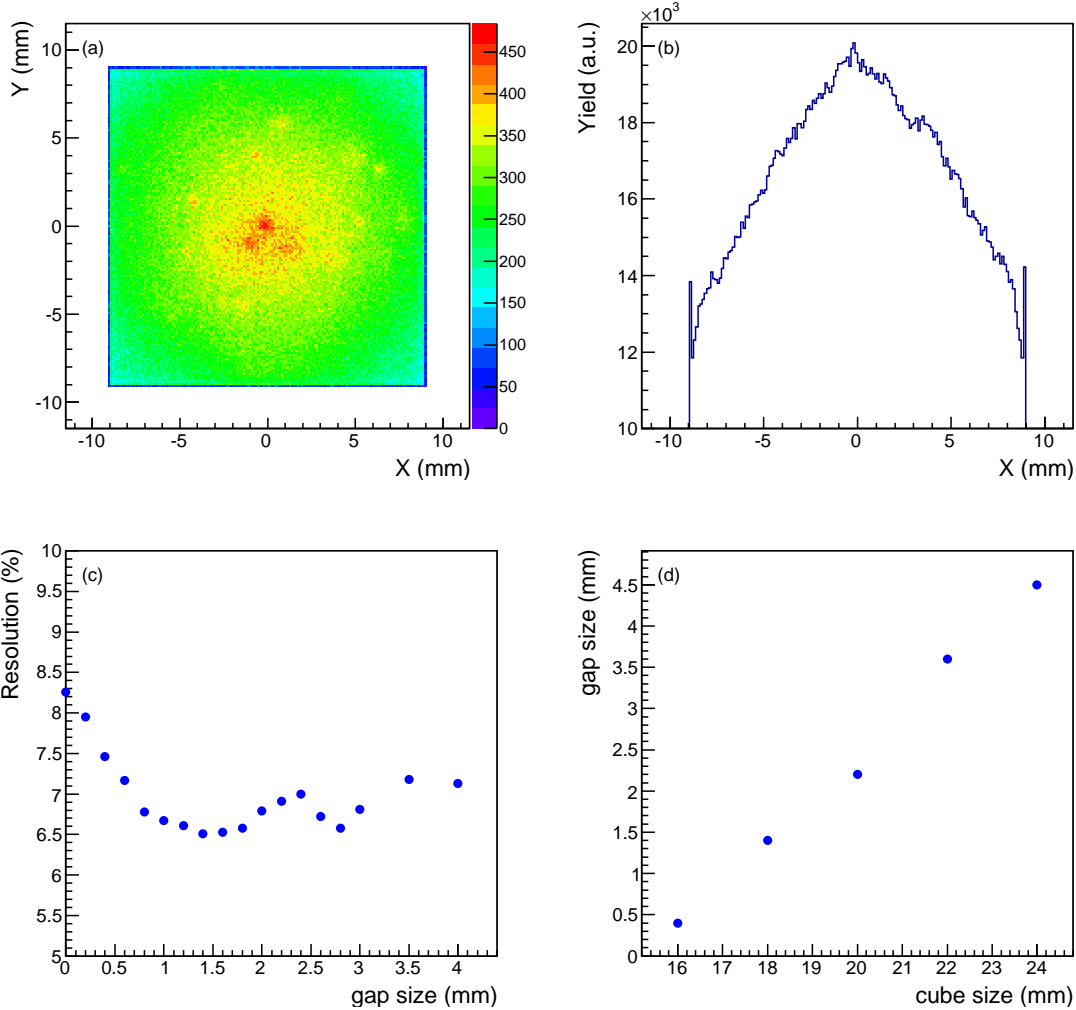


Fig. 1. Results of Geant4 simulations. (a) Distribution of scintillation photons at the exit of an 18 mm cubic scintillator irradiated by a 622 keV γ -ray located 20 cm away. (b) The profile of scintillation photon distributed in a 6 mm horizontal strip across the middle of the exit surface of the scintillator. (c) The detector resolution as a function of the gap size between the active area of SiPMs for a cubic NaI scintillator with 18 mm sides. (d) The gap size between the active area of SiPMs for scintillator cubes achieving an optimum energy resolution.

III. TEST OF SCINTILLATION DETECTORS

A SiPM array with four 6×6 mm² SiPMs [4] has been constructed following the analysis of the Geant4 simulations. Three types of scintillators, NaI, CsI, and Cs₂LiYCl₆:Ce³⁺ (CLYC), have been tested with this SiPM array. The scintillator and SiPM array were enclosed in a hermetically sealed aluminum container to keep out moisture and ambient light. All the tests were performed in a temperature controlled chamber.

A. Detector Response

The three detectors were tested using a ¹³⁷Cs source with the SiPMs biased at 27.5 V so that the detectors had the same nominal gain. The output of the preamp was recorded by a waveform digitizer (Struck SIS3302) operating at 100 MHz. The response of the detectors to the 662 keV γ -ray from ¹³⁷Cs was compared by making a histogram of the integral of the digitized pulses. Because the CLYC pulse has a long-decay

component, an integration time of 20 μ s was used for all the scintillators in order to make an unbiased comparison. Consequently, the counting rate was kept low to minimize pulse pileup. As the decay time for NaI and CsI is shorter, integrating these pulses for such a long time could introduce noise to the integrals. Since the comparison was for the detector response, the influence of noise on energy resolution was ignored for the current test. A separate measurement using the proper integration time for each scintillator was carried out to compare the energy resolution.

Figure 3 shows the normalized histogram of 10,000 pulse integrals for the three detectors. The NaI detector has the largest output because the SiPM response is optimized for the 420 nm scintillation photon. Although CsI has a larger yield of scintillation photons, the detector response is actually smaller than NaI. This is due to the mismatch between the scintillation spectrum of CsI and the response of the SiPMs. Lastly, the light output for CLYC is almost one half of that for NaI. Therefore, the pulse integral is the smallest.

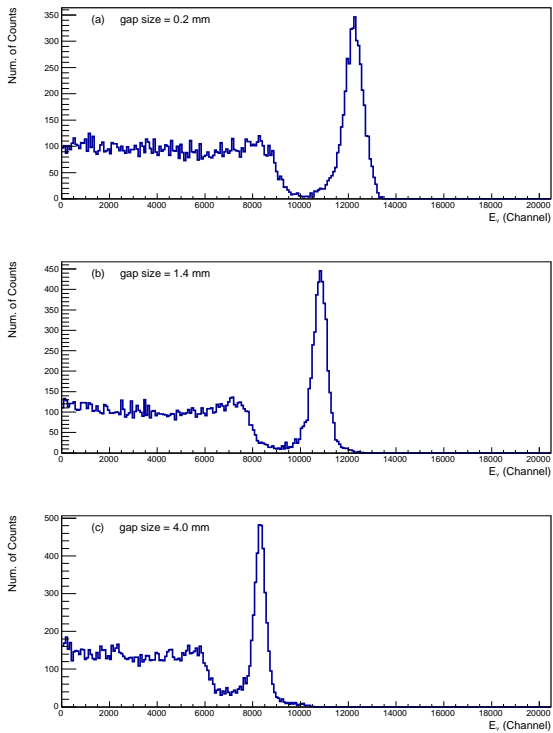


Fig. 2. Simulated spectra of a 662 keV γ -ray detected by an 18 mm cubic scintillator coupled to a 2x2 SiPM array. The gap size between the SiPMs is (a) 0.2, (b) 1.4, and (c) 4.0 mm.

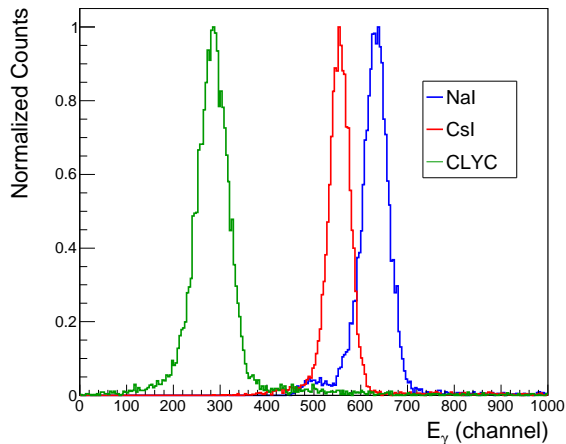


Fig. 3. The 662 keV photopeak of ^{137}Cs detected by the NaI, CsI, and CLYC detectors. The histograms are obtained by integrating the pulses of the preamp output for 20 μs .

B. γ -ray Detection

The breakdown voltage for the SiPMs varies individually due to the manufacturing processes. The breakdown voltage also increases with temperature which results in gain variation following temperature changes. In order to optimize the detector resolution, the gain for the SiPMs was adjusted to be the same within the array. Furthermore, the gain for the entire SiPM array was stabilized over the temperature range between -20 and 50 $^{\circ}\text{C}$ [5]. To check the quality of temperature

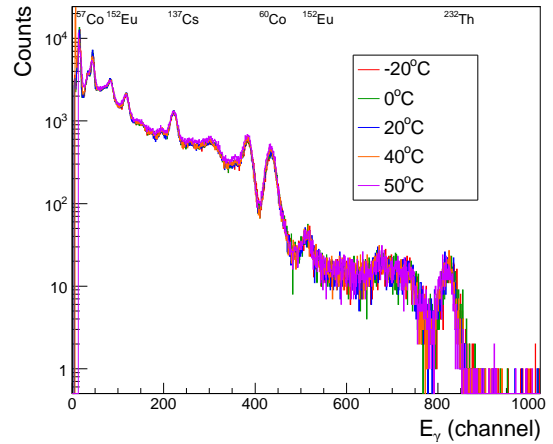


Fig. 4. Histograms of γ -rays from ^{152}Eu , ^{60}Co , ^{137}Cs , and ^{232}Th sources detected by the CsI detector at -20 , 0 , 20 , and 50 $^{\circ}\text{C}$.

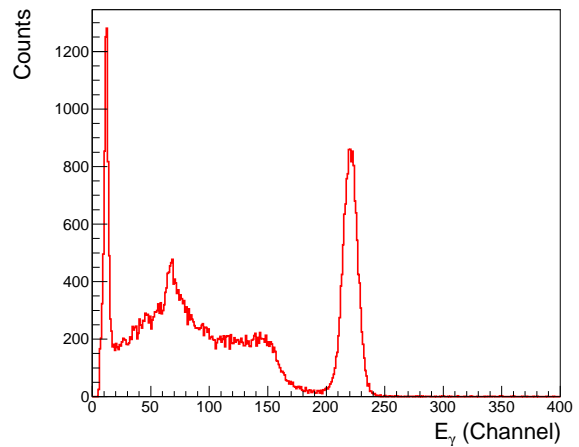


Fig. 5. Spectrum of ^{137}Cs γ -rays detected by the CsI detector. The gain of the SiPMs in the array has been matched to achieve an optimum energy resolution of 6.4%.

stabilization, γ -ray sources, ^{152}Eu , ^{60}Co , ^{137}Cs , and ^{232}Th , were used. Fig. 4 shows the spectra for these sources for the CsI detector at -20 , 0 , 20 , and 50 $^{\circ}\text{C}$. The centroid of the 662 keV photopeak for ^{137}Cs was set to channel 220 for all the temperatures. As can be seen, the location of the photopeaks do not shift for different temperatures because of the stabilization performed for the detector.

To optimize the energy resolution, the preamp output was integrated for 1, 4, and 20 μs for NaI, CsI, and CLYC, respectively. The best resolution obtained was 6.8% for NaI, 6.4% for CsI, and 7.8% for CLYC. It has been reported that an energy resolution of 4% was observed for a 1 cm^3 CLYC scintillator coupled to a PMT. However, when the same CLYC scintillator was coupled to SiPMs the energy resolution was between 6.2% and 8.3% [7]. The ^{137}Cs γ -ray spectrum measured by the CsI detector at 20 $^{\circ}\text{C}$ is shown in Fig. 5. The noise is sufficiently low such that the 32 keV peak is clearly visible without contamination.

The energy resolution of the 662 keV photopeak for CsI

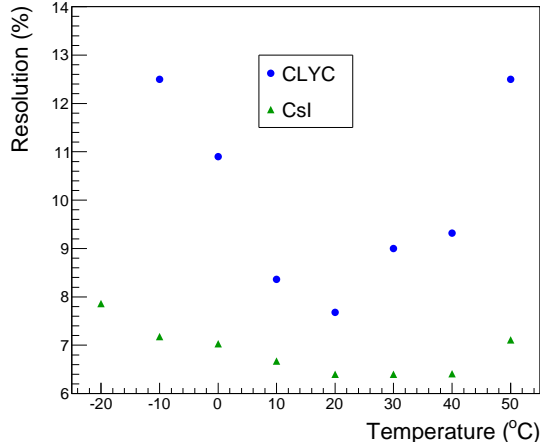


Fig. 6. (a) Energy resolution for CsI and CLYC detectors as a function of temperature.

and CLYC measured between -20 and 50 °C is displayed in Fig. 6. The variation in energy resolution for the CsI detector is small. At high temperatures, the poorer resolution is likely due to noise in the SiPMs whereas at low temperatures the poorer resolution is attributed to a lower light yield of the scintillator. For the CLYC detector, the energy resolution is much worse than that for CsI, particularly well below and above room temperature. At -20 °C, the 662 keV photopeak is barely visible in the γ -ray spectrum. A previous study using a smaller crystal, 1 cm³, obtained mixed results for resolution as a function of temperature [7]. In that study, SiPMs from different manufacturers were compared. For the SensL SiPM, the variation of energy resolution with temperature is smaller as compared to the present work. For the Hamamatsu SiPM, resolution as poor as 14% was measured at 10 °C. Since CLYC crystals are known to be fragile, it is conceivable that fractures might have developed in the crystal that was used in this work. This makes the use of CLYC for portable radiation detectors challenging because these instruments are required to operate between -20 and 50 °C.

In addition to studying the three detectors, a large number of CsI detectors have been tested which allow for examining the characteristics of the SiPMs. Fig. 7(a) shows the distribution of the breakdown voltages for 300 SiPMs. The standard deviation of the distribution is 0.124 V which is consistent with the manufacturer's specification. Fig. 7(b) shows the distribution of the temperature coefficient for the CsI detector. The centroid of the distribution is 15 mV/°C. In contrast, according to the manufacturer, the temperature coefficient for the SiPM alone is 21.5 mV/°C.

C. Neutron Detection

A ^{252}Cf source was used for studying neutron detection by the CLYC detector between -20 and 50 °C. According to the specification, the neutron is expected at 3.2 MeV in the γ -ray spectrum [6]. Since ^{232}Th has a 2.6 MeV γ -peak, it was used along with ^{252}Cf to test n- γ discrimination and as a reference for the energy spectrum. Because the largest



Fig. 7. (a) Distribution of the breakdown voltage for 300 SiPMs. (b) Distribution of the temperature coefficient.

difference in the pulse shape occurs in the first 2 μs , a shorter integration time of 4.5 μs , instead of 20 μs , was used to speed up the data acquisition. Fig. 8 shows the γ -ray spectrum detected by the CLYC detector. The photopeak for the ^{232}Th 2.6 MeV γ -ray appears near channel 2600 and the neutron peak appears near channel 3200. This agrees with the manufacturer's specification [6]. As can be seen, the neutron distribution is fairly broad and overlaps with the high-energy tail of the 2.6 MeV γ -peak. For this reason, it is necessary to use pulse-shape discrimination (PSD) to separate neutrons from γ 's.

The PSD is performed by taking the ratio of the pulse integral in the delayed window to the sum of the pulse integral in the prompt and delayed windows,

$$PSD\ Ratio = \frac{Delay}{Prompt + Delay}. \quad (1)$$

Shown in Fig. 9(a) is the histogram for the PSD ratio versus the integral of the preamp pulses. Neutrons appears in the group of counts in the upper-right corner. The band of counts located across the center of the histogram are γ -rays. The threshold for detection was set around 1.5 MeV to reduce the counting rate. The group of events near the end of the γ band on the right-hand side is the 2.6 MeV γ peak from ^{232}Th .

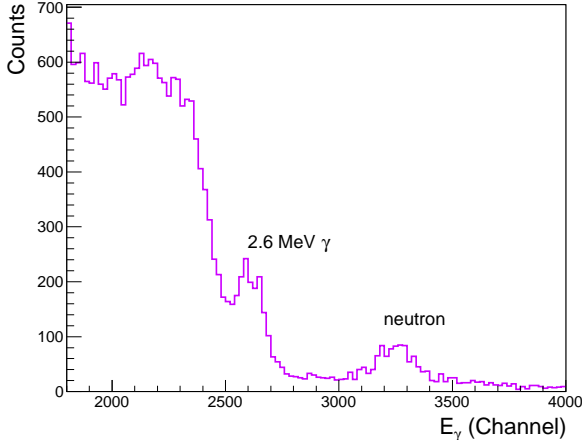


Fig. 8. Spectrum of γ -rays from ^{232}Th and neutrons from ^{252}Cf detected by the CLYC detector.

By projecting the two-dimensional histogram on to the vertical axis, the histogram of the PSD ratio is obtained, as shown in Fig. 9(b). The figure-of-merit (FOM) for PSD is defined as the ratio of the difference between the centroid (μ) of the γ and neutron peaks to the sum of the full-width-at-half-maximum (W) of the two peaks [7],

$$FOM = \frac{\mu_n - \mu_\gamma}{W_n + W_\gamma}. \quad (2)$$

The width for the prompt window and delayed window was varied to search for the best FOM. At 20 °C, the best FOM for n- γ discrimination is 1.9 for the width of the prompt and delayed window of 270 and 850 ns, respectively. The FOM increases with decreasing temperature due to the change of pulse shape. At 50 °C the FOM is 1.2 and at -20 °C the FOM is 3.0, as shown in Fig. 10. Although the resolution for CLYC is poor at the extreme temperatures, the neutron identification by pulse-shape discrimination works well.

IV. CONCLUSION

The NaI and CsI scintillation detectors constructed with the custom SiPM array have a good energy resolution for the 662 keV γ -ray from ^{137}Cs . They are suitable for deploying in a spectroscopic personal radiation detector (SPRD) such as the FLIR identiFINDER R200. Using pulse-shape discrimination, neutrons can be identified without contamination from γ -rays for the CLYC detector. However, the resolution for γ -ray detection is poor at extreme temperatures, -20 and 50 °C. Further work is in progress to find solutions for neutron detection in hand-held radiation detection instruments.

REFERENCES

- [1] P. Eckert, H.-C. Schultz-Coulon, W. Shen, R. Stamen, and A. Tadday, *Nucl. Instrum. Meth. A*, Vol. 620, No. 2-3, pp. 217-226, Apr. 2010.
- [2] S. Agostinelli *et al.*, *Nucl. Instrum. Meth. A*, Vol. 506, No. 3, pp. 250-303, July 2003.
- [3] M. Janecek and W.W. Moses, *IEEE Trans. Nucl. Sci.*, Vol. 57, No. 3, pp. 964-970, 2010.
- [4] MicroFC-60035, SensL Technologies Ltd.
- [5] Patent pending.

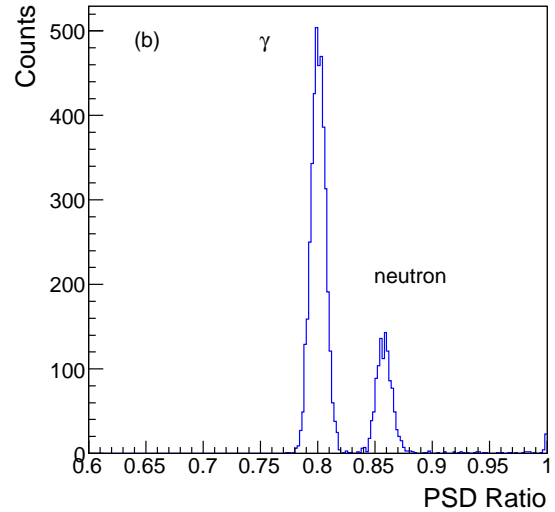
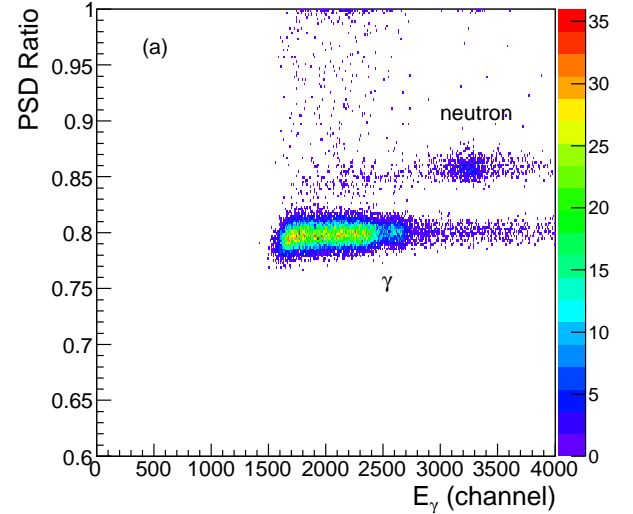


Fig. 9. (a) Histogram of PSD ratio versus pulse integral for the CLYC detector. Two radiation sources, ^{252}Cf and ^{232}Th , were present during the measurement. (b) Histogram of projected PSD ratio.

- [6] rmdinc.com/wp-content/uploads/2014/10/CLYC-Properties-PDF.pdf
- [7] K.E. Mesick, L.C. Stonehill, J.T. Morrell, D.D.S. Coupland, *2015 IEEE NSS/MIC, San Diego, CA, 2015*, pp. 1-4.

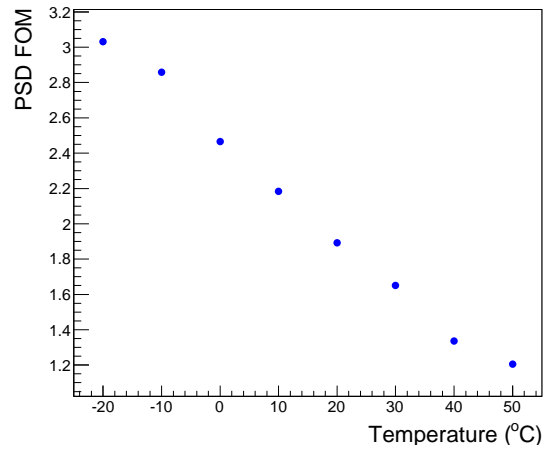


Fig. 10. The FOM of PSD for the CLYC detector as a function of temperature.